ARTICLE

Experimental and Theoretical Investigations of the Thermodynamic Stability of Ba−C_{60} and K−C_{60} Compound Clusters

Eva Zurek,[†,#,*] Jochen Autschbach,[‡] Nikola Malinowski,[§,▽] Axel Enders,[⊥] and Klaus Kern[∥,⊗]

[†]Max-Planck-Institut für Festkörperforschung, Heisenbergstrasse 1, 70569, Stuttgart, Germany, [‡]Department of Chemistry, State University of New York at Buffalo, Buffalo, New York 14260-3000, [§]Max-Planck-Institut für Festkörperforschung, Heisenbergstrasse 1, 70569, Stuttgart, Germany, [⊥]Department of Physics and Astronomy, University of Nebraska, Lincoln, Nebraska 68588, and [∥]Max-Planck-Institut für Festkörperforschung, Heisenbergstrasse 1, 70569, Stuttgart, Germany. [#]Current address: Cornell University, Department of Chemistry and Chemical Biology, Ithaca, New York 14853-1301. [▽]Permanent address: Central Laboratory of Photoprocesses, Bulgarian Academy of Sciences, 1040 Sofia, Bulgaria. [⊗]Alternate address: Institut de Physique des Nanostructures, Ecole Polytechnique Fédérale de Lausanne (EPFL).

ABSTRACT A novel experimental set-up was used to study superstable (magic) Ba−C_{60} and K−C_{60} compound clusters. The most stable systems observed cannot be rationalized by simple electronic or by geometrical shell filling arguments. Annealing the clusters past the temperature necessary for the fragmentation of the initial metastable clusters formed at the source reveals information about their thermodynamic stability. Higher temperatures yield larger species, suggesting that similar experiments may be used to rationally produce nanoscale clusters with highly desirable properties. Density functional calculations reveal ionic (K, Ba) and covalent (Ba) bonding between C_{60} and the metal atoms. The entropic contribution to the Gibbs free energy is shown to be essential in determining absolute and relative cluster stabilities. In particular, we demonstrate that at higher temperatures the entropy favors the formation of larger clusters. A simple criterion which may be used to determine the absolute and relative stabilities of general multicomponent clusters is proposed.

KEYWORDS: magic clusters · fullerenes · density functional calculations · cluster stability · chemical bonding

*Address correspondence to e.zurek@fkf.mpg.de, ez56@cornell.edu.

Received for review January 11, 2008 and accepted April 07, 2008.

Published online May 10, 2008.
10.1021/nn800022d CCC: $40.75

Recently, a tremendous amount of experimental and theoretical effort has been directed toward the study of clusters due to their potential applications in nanotechnology.[1−6] For example, chemically inert clusters may be ideal building blocks for tailored nanomaterials. Thus, it is important to uncover general principles which may be used to explain enhanced cluster stability and to understand how the experimental conditions affect which superstable (magic) clusters are produced.

Often, geometric and electronic shell filling arguments can adequately explain the pronounced stability of so-called magic clusters. For example, the stability of $Ba_{32}C_{60}$ was attributed to geometrical shell filling.[7] It was postulated that each Ba atom is situated on top of one of the 12 pentagonal or 20 hexagonal faces of the fullerene and that completion of this first metallic layer leads to increased stability. On the other hand, the stability of $(K_6C_{60})_nK^+$ was explained *via* electronic shell-filling arguments.[8] The C_{60} LUMO is triply degenerate and can therefore accommodate six electrons. Thus, a transfer of the valence $4s^1$ occupations from six potassium atoms yields a particularly stable structure. The coincident closure of both the electronic and geometric shells accounts for the magic character of the Al_{13}^- cluster anion.[9] Other examples where both factors play a role include $AlPb_{10}^+$, $AlPb_{12}^+$[3] and $Sc@Cu_{16}^+$.[4] The first two systems adopt a close-packed structure with optimally filled electronic shells, whereas the third exhibits a closed electronic shell along with a highly stable dopant encapsulated structure. However, recent studies have pointed out that simple geometric and electronic shell-filling arguments may not be generally applicable to determine which clusters are magic.[1,2]

In a recent communication on metal–fullerene clusters we have demonstrated that the experimental setup drastically affects the observed cluster distribution.[1] In the experiments of Martin *et al.*,[7,8] the clusters were produced in a low-pressure, inert gas condensation cell cooled by liquid nitrogen. After being transported to a high vacuum chamber they were photoionized. To enhance the intensity of the magic peaks it was necessary to heat the clusters either with the same laser pulse used for ionization or with a second pulse which arrived after the ionizing laser. A new experimental setup containing a novel heating/cooling

stage mounted directly after the cluster source has revealed a different set of magic peaks for Ba−C_{60} and K−C_{60} compound clusters.[1] Here, the clusters were heated to a temperature varying between 150 to 1800 K *via* thermalization with a He bath for a time span on the order of *ca.* 1 ms. Afterward, they were cooled to 150 K then photoionized and measured by time-of-flight (TOF) mass spectroscopy. Since photon absorption occurs within nanoseconds, it was postulated that the clusters produced by Martin *et al.* may not be the most stable configurations. The new experimental setup overcomes this: the longer annealing times increase the probability to reach the minimum in the Gibbs free energy (GFE). Indeed, our density functional calculations revealed that entropy plays a substantial role in determining absolute cluster stability and that the experimentally observed magic clusters corresponded to minima in the GFE.

Herein, we illustrate how the temperature of the heating stage affects the observed distribution of Ba−C_{60} and K−C_{60} compound clusters. Our results suggest that the experimental setup may be used to produce nanoscale clusters with a set of specific, desirable properties simply by modifying the annealing temperature. By monitoring the mass spectra and decay curves obtained at different temperatures of the heating stage, we demonstrate that the thermodynamic stability of the clusters is probed at temperatures surpassing those required for fragmentation of the initial metastable clusters formed at the source. Moreover, we show that the experimental setup measures the stability of the neutral, and not of the charged, species. Density functional calculations are employed to uncover the most stable $M_n(C_{60})_2$ (M = K, Ba; $1 \leq n \leq 6$) systems and to explain the origin of their stability. Finally, a simple criterion which may be used to determine the absolute and relative stabilities of multicomponent clusters, where the quantity of only one of the components changes, is proposed.

EXPERIMENTAL RESULTS

Thermal Stability of C_{60}−Ba Clusters. Previously, we have demonstrated that the thermal stability of C_{60} clusters can be significantly enhanced by adding alkali or alkaline-earth metal atoms, thus forming superstable metal—$(C_{60})_m$ compound clusters.[1] Whereas the decay temperatures for $(C_{60})_2$, $(C_{60})_3$, and $(C_{60})_4$ were found to be 189, 270, and 340 K, respectively, much higher annealing temperatures could be reached *via* addition of K or Ba. Figure 1 illustrates the effect of the temperature of the heating cell on the mass spectra of $Ba_n(C_{60})_m$ clusters (in all cases the cooling cell was maintained at 150 K). Examination of Figure 1a reveals that the "cold" spectrum obtained at 150 K appears smooth, with no pronounced peaks, as is characteristic for a statistical size distribution. Figure 1b illustrates that as the temperature is raised to 1280 K, distinct peaks start to arise. At 1780 K, several prominent peaks corresponding to particularly stable configurations are found (see Figure 1c). These $Ba_n(C_{60})_m$ magic clusters have the configuration $(n, m) = (3, 2), (5, 3), (7, 4), (10, 5), (13, 6)$, and $(14, 7)$. Further annealing only leads to entire groups of peaks gradually disappearing from the mass spectrum. Clearly, the heating method influences which clusters are detected, as none of the peaks correspond to those observed in ref 7. Moreover, neither geometric nor electronic shell-filling arguments can explain the stable configurations which are observed and the significantly enhanced stability of the clusters. Shell-filling arguments would predict that, for example, $Ba_{64}(C_{60})_2$ or $Ba_6(C_{60})_2$ are magic. Our experimental results indicate that different sets of magic clusters may be obtained by tuning the temperature and dwell time of the clusters inside the heating stage. This could prove to be very

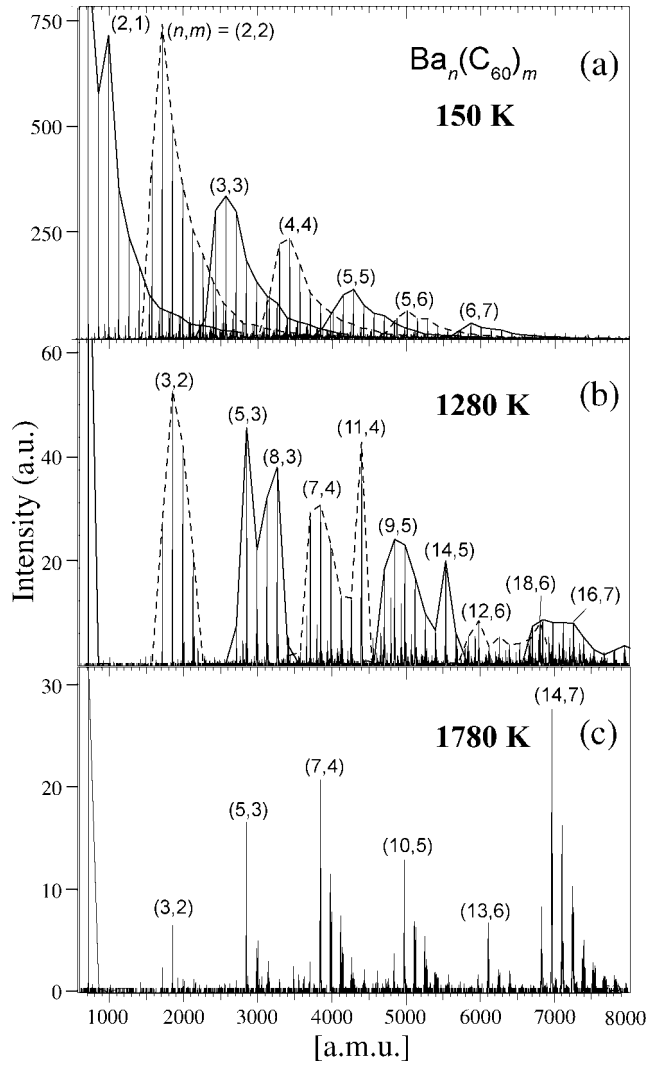

Figure 1. TOF mass spectra of $Ba_n(C_{60})_m$ clusters obtained (a) without annealing the cluster beam in the heating cell (T = 150 K); (b) after annealing the cluster beam to T = 1280 K; (c) after annealing the cluster beam to T = 1780 K. Mass peaks are labelled according to (n, m) where n is the number of barium atoms and m is the number of C_{60}s.

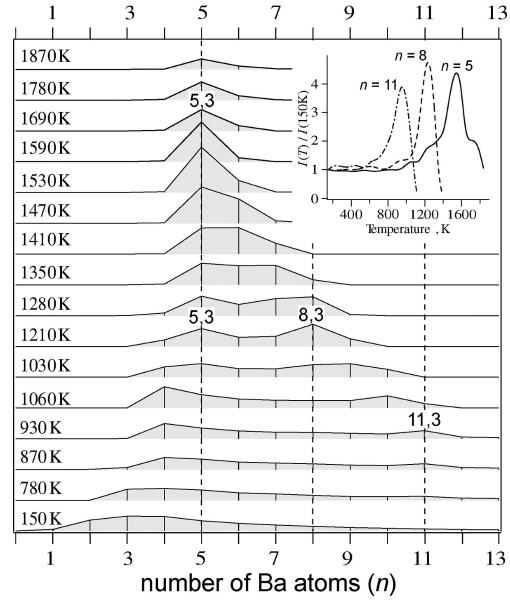

Figure 2. Evolution of the peak intensities of $Ba_n(C_{60})_3$ clusters with annealing temperature. The intensities of the peaks have been normalized to the signal accumulation time as well as to the integrated intensities of the signal in the mass range from 1460 to 20000 amu. At high temperatures the most thermodynamically stable species is $(n, m) = (5, 3)$. At intermediate temperatures, below 1300 K, (8, 3) is also found to be thermodynamically stable. The thermal decay curves for the three prominent configurations with 5, 8, and 11 barium atoms are shown in the inset. The abundance of these clusters assumes a maximum for temperatures just below the decay temperature.

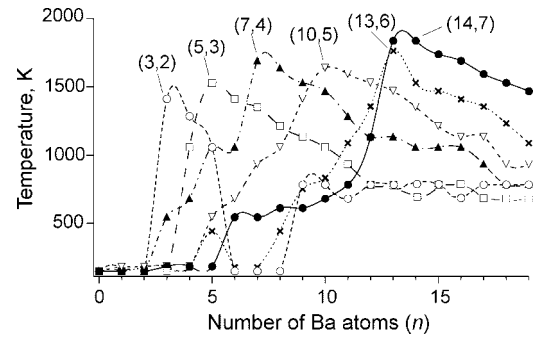

Figure 3. Temperatures at which the abundance of $Ba_n(C_{60})_m$ clusters assumes a maximum. See Figure 2 for definition.

useful for the design of nanoscale clusters with, for example, highly desirable optical or magnetic properties. However, thermal equilibration is necessary to produce clusters with the most stable configurations. Metastable structures can easily be created by nonequilibrated cluster beams.

To follow the thermally induced structural transition, we have taken a series of mass spectra, gradually adjusting the temperature of the heating stage. In Figure 2 we illustrate the dependence of the position and intensity of the peaks for $Ba_n(C_{60})_3$. The intensities of the mass peaks have been normalized here to the signal accumulation time as well as to the integrated intensities of the signal in the mass range from 1460 to 20000 amu, to allow for a direct comparison of the intensities. At 150 K, a broad distribution with $1 \leq n \leq 13$ is found. The initial heating stages probe the *kinetic* stability of the clusters formed at the source. That is, we need to overcome the activation energy necessary for these metastable clusters to fragment. Our experiment yields information about the *thermodynamic* stability of the $Ba-C_{60}$ clusters only after complete fragmentation of the initial compounds has occurred. Thermodynamic equilibrium is achieved through the long annealing times (~1 ms). Examination of Figure 2 illustrates clearly that at 1210 K $Ba_8(C_{60})_3$ and $Ba_5(C_{60})_3$ are thermodynamically the most stable species. If they were only kinetically stable then one would expect the peaks at 150 K to be at least as intense as those at 1210 K. Instead, the height of these signals increases with increasing temperature. Further annealing results in the disappearance of $Ba_8(C_{60})_3$ from the mass spectra and a sharp increase in the amount of $Ba_5(C_{60})_3$, which displays a maximum at 1530 K.

In an equilibrium mixture at constant temperature and pressure, the most stable clusters minimize the GFE. Later, we will demonstrate that for this set of systems the entropic contributions to the GFE are considerable and play a substantial role in determining which clusters are magic. Annealing past 1530 K results in the gradual decay of $Ba_5(C_{60})_3$, until it has almost disappeared (*i.e.*, it is no longer a minimum on the GFE surface) at around 1870 K. The decay curves for $Ba_5(C_{60})_3$, $Ba_8(C_{60})_3$, and $Ba_{11}(C_{60})_3$ in the inset of Figure 2 illustrate that for systems containing $3C_{60}$s, the higher the temperature, the lower the amount of Ba atoms in the most thermodynamically stable species. However, examination of Figure 1 reveals that in general higher temperatures shift the equilibrium toward larger clusters. For example, $Ba_3(C_{60})_2$ clusters assume an intensity maximum at 1280 K, whereas the larger $Ba_{14}(C_{60})_7$ clusters are most abundant at 1780 K. This is also seen clearly in Figure 3 which illustrates that of all clusters containing $(C_{60})_m$ ($m < 8$) the $Ba_{14}(C_{60})_7$ clusters have the highest decay temperatures. Figure 3 also shows that the greater the amount of fullerenes in the cluster, the greater the number of bariums necessary for thermal stabilization, suggesting that the clusters contain $C_{60}-Ba-C_{60}$ bonds.

To determine if the magic configurations are dependent upon the charge, we have also investigated the abundance spectra of multiply charged clusters. By focusing the light of the ionization laser with a lens the probability of multiphoton ionization of clusters was increased and hence larger amounts of doubly charged clusters were produced. Mass spectra of singly and doubly charged $Ba_n(C_{60})_3$ clusters are shown in Figure 4. The doubly charged clusters appear at one-half of the mass of singly charged clusters. There is quantitative agreement between the peak intensities of singly and doubly charged clusters, and the isotopic distribution, shown for the (5, 3)-cluster in the inset, coincides quan-

titatively with the simulated intensities for this configuration (bars in the inset). It can be concluded from this agreement that the magic cluster configuration does not depend on the cluster charge. Thus, our experiments probe the stability of the *neutral* clusters.

In summary, heating to moderate temperatures yields information about the kinetic stability of the initial metastable clusters formed at the source. When the temperatures are high enough to overcome the activation barrier for the fragmentation of these metastable clusters, our experiments probe the thermodynamic stability of the Ba$-$$C_{60}$ compound clusters.

Thermal Stability of $C_{60}$$-$K Clusters. To distinguish further between electronic and geometric effects, we substituted Ba by K in the experiments. K has a similar ionic radius as Ba (r_{Ba^+} = 1.53 Å, $r_{Ba^{2+}}$ = 1.34 Å, r_{K^+} = 1.33 Å) but only half as many valence electrons (Ba: [Xe]6s^2; K: [Ar]4s^1). Thus, identical magic numbers as for the Ba$-$$C_{60}$ clusters would be an indication that geometric effects determine the stability of these systems. Figure 5 illustrates that at 900 K the most stable $K_n(C_{60})_m$ clusters had the composition (n, m) = (4, 2), (6, 3), (8, 4), (11, 5), (14, 6), and (17, 7), none of which were observed in ref 8. Once again, the experimental conditions have an influence on the magic peaks observed, and neither electronic nor geometric shell-filling arguments can be used to rationalize the species produced. The former and latter would predict, for example, that $K_{12}(C_{60})_2$ or $K_{64}(C_{60})_2$ are particularly stable structures. Here, thermal equilibration is also necessary in order to fragment all of the initial metastable clusters formed at the source and probe the thermodynamic stability of the K$-$$C_{60}$ systems. Whereas annealing the K$-$$C_{60}$ clusters past 900 K led to the disappearance of whole groups of peaks from the mass spectrum, the Ba$-$$C_{60}$ species could be heated up to *ca.* 1900 K, indicating that the latter exhibit stronger metal—fullerene bonding than the former.

Figure 6 illustrates that once the fragmentation of the metastable clusters formed at the source is complete, a complex thermodynamic equilibrium is reached. In complete agreement with the results obtained for Ba$-$$C_{60}$, larger clusters appear to be thermodynamically more stable than smaller ones at very high temperatures. For example, $K_{17}(C_{60})_7$ and $K_{14}(C_{60})_6$ have the highest decay temperatures.

For the $K_n(C_{60})_m$ clusters, we have also investigated the dependence of the stable cluster configurations on the cluster charge, similar to the procedure described earlier. We can conclude here also that our experiments probe the stability of neutral clusters, as we did not observe a charge dependence of the spectra of the stable cluster configurations.

THEORETICAL RESULTS

Ba_nC_{60} and K_nC_{60} Clusters. Despite the fact that theoretical work on exohedral fullerene clusters is abundant,

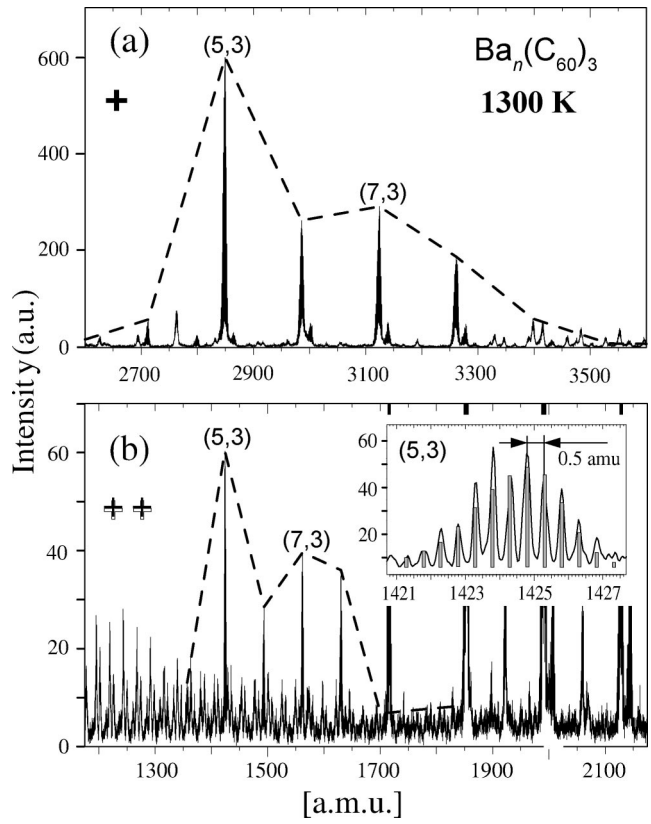

Figure 4. Abundance mass distribution of (a) singly and (b) doubly charged $Ba_n(C_{60})_3$ clusters at an annealing temperature of 1300 K. (Panel b inset) High-resolution measurement of the isotopic distribution of the doubly charged (5, 3) cluster, together with the simulated isotopic distribution (bars).

only a few papers specifically consider a single C_{60} with a varying number of K atoms. Electronic structure calculations have been performed on K_nC_{60} with n = 1, 2, 3;[10,11] n = 6, 12[11] and n = 32.[12] To the best of our knowledge, there has not been any previous computational work on Ba containing clusters, however DFT has been used to study Ca_nC_{60}, with n = 12, 20[13] and n = 32.[12,13] Recently, quantum chemical molecular dynamics simulations have been successfully used to study the mechanism of fullerene formation.[14]

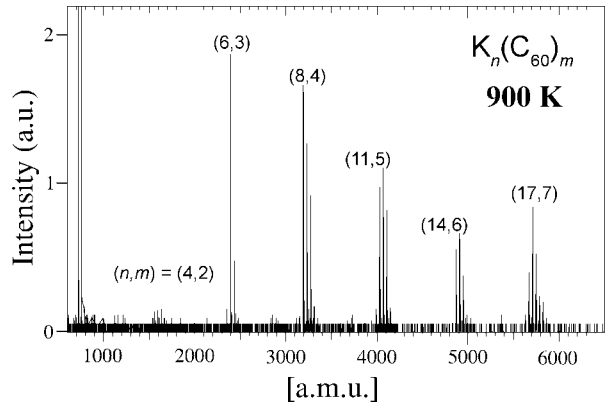

Figure 5. TOF mass spectra of $K_n(C_{60})_m$ clusters obtained after annealing the cluster beam to T = 900 K. Mass peaks are labelled according to (n, m) where n is the number of potassium atoms and m is the number of C_{60}s.

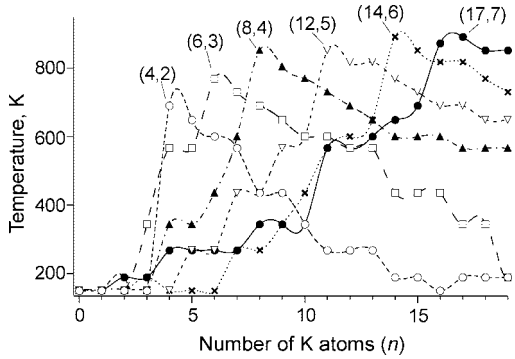

Figure 6. Temperatures at which the abundance of $K_n(C_{60})_m$ clusters assumes a maximum.

Herein, we will consider the general reaction

$$nM + mC_{60} \rightarrow M_n(C_{60})_m \quad (1)$$

where M = K, Ba and $m = 1, 2$. We define the bonding energy per metal atom, Δ_M^E, as

$$\Delta_M^E = \frac{E(M_n(C_{60})_m) - nE(M) - mE(C_{60})}{n} \quad (2)$$

where $E(x)$ is the energy of species x . The change in the Gibbs free energy per metal atom, Δ_M^G, finite temperature enthalpy correction per metal atom, $\Delta_M^{H_{EC}}$, and the entropy per metal atom multiplied by the temperature, $T\Delta_M^S$, will be defined similarly to the Δ_M^E in eq 2 for the reaction given in eq 1. Within the Appendix we illustrate that for a set of binary clusters A_nB_k with varying n, a comparison of Δ_A^W, where W is the energy, enthalpy, Gibbs or Helmholz free energy, easily and unambiguously reveals the absolute and relative stabilities of the clusters within the set. The Cartesian coordinates and energies of all of the systems studied are given in the Supporting Information.

The geometries of five possible isomers of MC_{60} (M = K, Ba) were optimized. The metal atom may lay on top of a hexagonal face (MC_{60}^{hex}), a pentagonal face (MC_{60}^{pent}), a carbon atom (MC_{60}^{atom}), a bond belonging to two hexagonal faces ($MC_{60}^{b_1}$) or a bond belonging to one hexagonal and one pentagonal face ($MC_{60}^{b_2}$) of the fullerene. We have not considered endohedral Ba/K@C_{60} systems since fragmentation experiments revealed that the metal atoms cannot be located inside the metal cages. However, a recent publication has studied heavy atoms in C_{60}.[15] Table 1 gives the Δ_M^E and Mulliken charges for these different structures. For both potassium and barium, the MC_{60}^{hex} isomer had the most negative Δ_M^E, in accordance with previous theoretical calculations for KC_{60}.[10,11] $MC_{60}^{b_2}$ (M = K, Ba) and BaC_{60}^{atom} are not stationary points and optimized to yield MC_{60}^{pent} and $BaC_{60}^{b_1}$, respectively. Examination of the charges reveals an almost full transfer of the $4s^1$ valence occupations from potassium to the fullerene LUMO. A full charge donation between the barium atom and C_{60} does not occur, as can be seen in the Mulliken charges of *ca*. 1.3. The magnitude of Δ_{Ba}^E was found to be somewhat larger than that of Δ_K^E, indicating that a Ba−C_{60} bond is slightly stronger than a K−C_{60} bond.

TABLE 1. The Δ_M^E (kcal/mol)[a] and Mulliken Charges of the Metal Atoms for Different Isomers of MC_{60} (M = K, Ba)

		M = K		M = Ba	
isomer	symmetry	Δ_K^E	charge	Δ_{Ba}^E	charge
MC_{60}^{hex}	C_s	−38.87	0.92	−43.75	1.31
MC_{60}^{pent}	C_s	−36.98	0.93	−38.14	1.31
MC_{60}^{atom}	C_s	−34.44	0.93		
$MC_{60}^{b_1}$	C_{2v}	−33.47	0.93	−40.78	1.27
$MC_{60}^{b_2}$	C_s				

[a] As defined in eq 2.

Hamamoto *et al*. have found that, for the most stable isomers of K_nC_{60} ($n = 1, 2, 6$) and $K_3C_{60}^-$, the potassium ions are located on top of the hexagonal fullerene faces. Moreover, to reduce the Coulomb repulsion, the potassium ions are as far apart from each other as possible.[11] With this in mind, we have optimized possible structures for K_nC_{60} ($1 \leq n \leq 6$), shown in Figure 7. Since it was not the main goal of this work to study clusters containing one fullerene, different geometric alternatives were not considered. Nonetheless, we can examine the Δ_K^E and average Mulliken charges per potassium for the optimized clusters, given in Figure 8a,b, respectively. In agreement with previous work,[10,11] the Δ_K^E becomes less negative and the charge per atom decreases, with increasing n . To decrease the Coulomb repulsion between the potassium ions, progressively less charge is donated to the C_{60} unoccupied orbitals as n increases. This implies a weaker ionic bonding, along with a decrease in the amount of energy gained upon cluster formation for larger n . However, as will be shown later, it is not the Δ_M^E, but the Δ_M^G, which in this case determines the most stable clusters.

We have also optimized possible isomers of Ba_nC_{60} ($n = 2, 3$), with the same configuration as the potassium

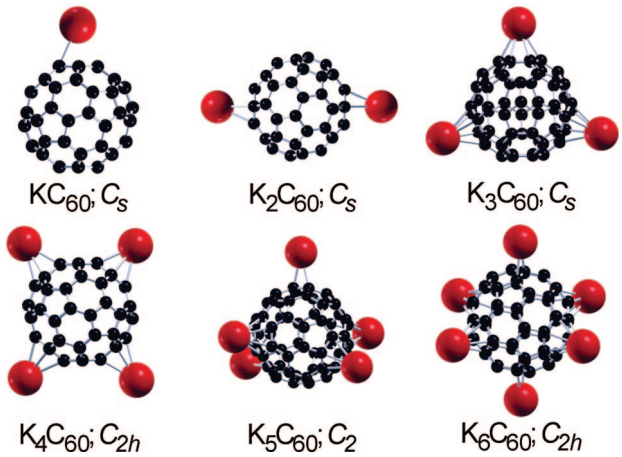

Figure 7. Optimized geometries and symmetries of the K_nC_{60} ($1 \leq n \leq 6$) clusters.

clusters shown in Figure 7. The Δ^E_{Ba} and average Mulliken charges per barium can be found in Figure 8c and 8d, respectively. The Δ^E_{Ba} for the barium clusters are *ca.* 5 kcal/mol larger in magnitude than for the potassium, indicating stronger C_{60}−Ba bonding. Once again, the average charge on the metal decreases with increasing *n*. In contrast to the potassium clusters, the structure with the lowest Δ^E_{Ba} contains two, not one, metal atoms. Interestingly, Ba_2C_{60} corresponds to a magic peak at 150 K in Figure 1a, indicating that this is a metastable cluster formed at the source.

From this initial study on potassium and barium interaction with C_{60}, we can conclude that both metals prefer to bond to a hexagonal fullerene face. However, the nature of the metal—C_{60} interaction is different in each case. For potassium, the bonding appears to be purely ionic with a decreasing amount of charge transfer to the C_{60} per K (and therefore a decreasing Δ^E_K), with increasing *n*. In the case of barium, the bonding is not completely ionic, as indicated by the relatively low metal atom charges. Another mechanism must be considered which also explains the minimum in Δ^E_{Ba} occurring for Ba_2C_{60}.

Bonding and Stability of $Ba_n(C_{60})_2$ ($1 \leq n \leq 6$) Clusters. The optimized geometries and Δ^E_{Ba} of possible $Ba_n(C_{60})_2$ ($1 \leq n \leq 6$) isomers are given in Figure 9. Due to the fact that irradiation of solid C_{60} with visible or ultraviolet light induces a [2 + 2] cycloaddition leading to the formation of C_{60} dimers,[16,17] we have considered structures containing a $(C_{60})_2$ carbon framework, **9.1** and **9.4**. Examination of the most stable $n = 1, 2$ clusters (**9.2** and **9.5**) shows that their Δ^E_{Ba} is much larger in magnitude (40−45 kcal/mol), indicating that a C_{60}-bridging−Ba bond is much stronger than the bond between two C_{60}s. It is also stronger than a Ba−C_{60} bond since the Δ^E_{Ba} of **9.2** is *ca.* 30 kcal/mol greater in magnitude than that of the most stable BaC_{60} isomer. Moreover, comparison of **9.6** and **9.8** reveals that the C_{60}-bridging−Ba bond is also more favorable than a Ba−Ba bond. The most stable structures for a given *n* all have a C_{60}−Ba_n−C_{60} arrangement, with the barium atoms sandwiched between the two fullerenes (set A). However, as *n* increases, the Δ^E_{Ba} of clusters with a Ba−C_{60}−$Ba_{(n-2)}$−C_{60}−Ba configuration (set B) becomes comparable. For example, the Δ^E_{Ba} of **9.11** is only 1.3 kcal/mol less negative than that of **9.12**. It must be noted that for the $Ba(C_{60})_2$ cluster belonging to set A, we have considered geometries where the barium atom was situated between two hexagonal rings (with D_{3d}, D_{3h}, C_{2v}, and C_{2h} symmetries), two hexagonal rings rotated 30° with respect to each other (D_3 and C_2 symmetries), two pentagonal rings (D_{5h} and C_{2v} symmetries) and two pentagonal rings rotated 27° with respect to each other (D_{5d} and C_{2h} symmetries). The D_{5h}, D_{5d}, D_{3h}, D_{3d}, and D_3 symmetries led to doubly degenerate half-filled HOMOs for which Δ-SCF singlet and triplet energies were considered, and geometry relaxation led

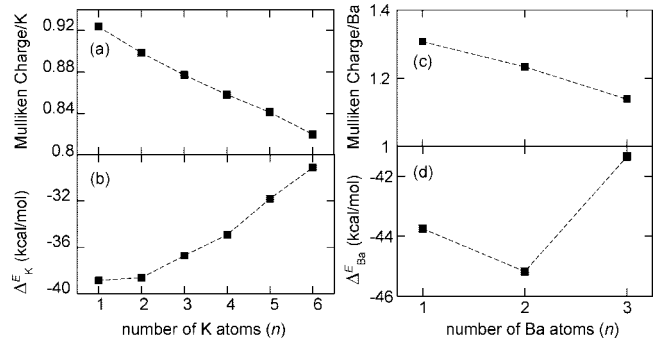

Figure 8. (a) Average Mulliken charges per K atom and (b) Δ^E_K of the K_nC_{60} ($1 \leq n \leq 6$) clusters; (c) average Mulliken charges per Ba atom and (d) Δ^E_{Ba} of the Ba_nC_{60} ($1 \leq n \leq 3$) clusters.

to lower symmetries with a closed-shell electronic structure (C_{2v}, C_{2h}, C_2). The energies of all of the structures were within *ca.* 7.5 kcal/mol of each other. However, the isomer lowest in energy contained a barium atom situated between two hexagonal rings and C_{2h} symmetry (**9.2**). Hence, in all of the subsequent starting geometries (except **9.1** and **9.4**) the two hexagonal faces of C_{60} were chosen to point toward each other. Configurations containing σ_h or σ_v symmetry operations were considered, and only the clusters with the lowest energy are shown in Figure 9.

To clarify the nature of the bonding for the most stable structural alternatives for a given *n* (**9.2**, **9.5**, **9.8**, **9.10**, **9.12**, and **9.14**) we first of all reoptimized

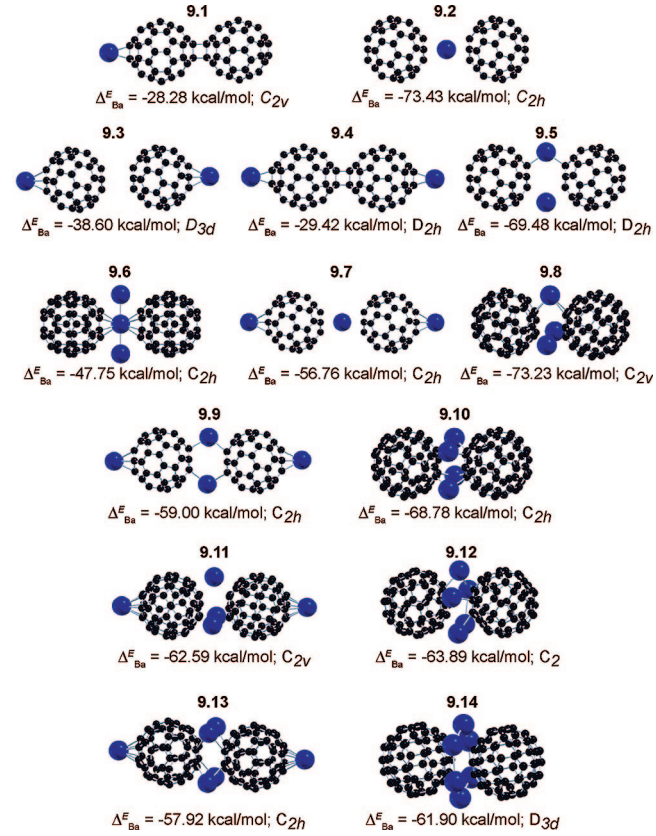

Figure 9. Optimized geometries and symmetries of the $Ba_n(C_{60})_2$ ($1 \leq n \leq 6$) clusters.

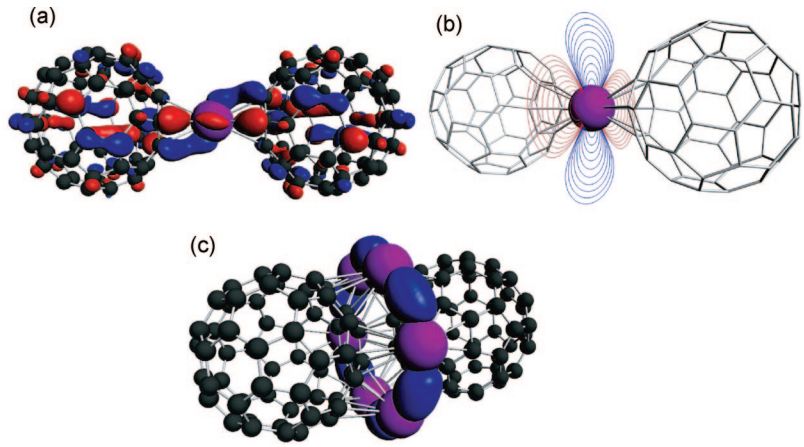

Figure 10. (a) The $Ba(C_{60})_2$ HOMO, isosurface = ±0.023 au. It is composed primarily of the LUMOs of the two fullerenes and contains some Ba $5d_{z^2}$ and $5d_{x^2-y^2}$ character. (b) A contour diagram of the $Ba(C_{60})_2$ HOMO taken in a plane passing through the Ba atom. (c) The $Ba_6(C_{60})_2$ HOMO-3, isosurface = ±0.031 au. It contains primarily Ba $5d_{yz}$, 6s, and some C_{60}-π* character. The Ba atoms are colored purple; C atoms black.

these geometries with a higher integration accuracy and then performed a fragment orbital analysis, using the distorted fullerenes (as found in the optimized cluster) and the free Ba atoms, as fragments.[18] This yielded the composition of the molecular orbitals of the metal-fullerene clusters in terms of the occupied and unoccupied orbitals of Ba and C_{60}. In $Ba(C_{60})_2$, all of the occupied orbitals, with the exception of the HOMO, were composed of occupied orbitals of the two distorted fullerenes, the Ba core and semicore orbitals, and in rare cases contained a small amount of Ba 5d character. The HOMO itself, on the other hand, was made up primarily of unoccupied C_{60} orbitals and contained some Ba $5d_{z^2}$ and $5d_{x^2-y^2}$ character (6% total). This shows that an important component of the bonding in the $Ba(C_{60})_2$ cluster originates from an electron transfer from the Ba 6s orbital to the LUMOs of the two fullerenes. However, despite the fact that one might expect a Ba^{2+} ion to be strongly stabilized when placed between the two negatively charged C_{60} moieties, a complete transfer of the two valence 6s electrons to the C_{60} unoccupied orbitals does not occur. This finding is supported by a calculated Mulliken charge of 1.60 on the Ba atom. Instead, we find back-donation into the empty Ba 5d orbitals leading to Ba-5d−fullerene bonding, which is seen clearly in Figure 10a. Thus, our results support the classification of Ba as an "honorary d-element" by Pyykkö *et al.*[19–21]

The Ba—C bond length of 3.06 Å in **9.2** can be compared with the Ba—N bond length of 2.65 Å calculated for the CsN_7Ba system in ref 19. The latter was shown to have up to quintuple bonds (σ, two π, and two δ). In Figure 10 the calculation has oriented the long axis of the molecule along the *x*-axis of the coordinate system due to the overall symmetry. A linear combination of the Ba $5d_{z^2}$ and $5d_{x^2-y^2}$ basis functions may give rise to σ or δ bonding contributions at the Ba center. δ-bonding d-orbitals for this orientation of the molecule would be d_{yz} and $d_{y^2-z^2}$. Projection of a $d_{z^2}-d_{x^2-y^2}$ linear combination with the same coefficients as calculated for the HOMO of **9.2** onto d_{yz} and $d_{y^2-z^2}$ yielded 0.000 and 0.186, respectively. The square of 0.186 divided by the sum of the square of the d_{z^2} and $d_{x^2-y^2}$ coefficients in the HOMO yields almost 99% showing that the Ba—fullerene backbonding in the HOMO is mainly a δ-type bond, as the contour diagram in Figure 10b reveals. Other occupied orbitals have slight contributions (1−2%) from Ba $5d_{xy}/d_{xz}$ and 6s orbitals which would lead to π and σ bonds in this orientation. Hence, **9.2** also affords σ, π, and δ Ba—C bonding analagous to CsN_7Ba.[19]

Our calculations also revealed that for $2 \leq n \leq 6$, the occupied orbitals, except for the *n* highest, were composed primarily of occupied C_{60} and Ba core and semicore orbitals (in some cases a small amount of Ba 5d character was also present). The *n* highest orbitals, on the other hand, were composed primarily of the C_{60} LUMOs, other unoccupied fullerene orbitals and also contained Ba 5d character. For $n = 5, 6$, some Ba 6s character could also be found. As *n* increases the Ba atoms become close enough to each other so that they may also form Ba−Ba bonds, leading to the formation of a metal cluster between the C_{60}s. For example, σ-bonding between nearest neighbor Ba atoms is evident in the HOMO-3 of $Ba_6(C_{60})_2$, shown in Figure 10c.

Our analysis illustrates that the $Ba_n(C_{60})_2$ clusters exhibit ionic bonding due to a transfer of the Ba 6s electrons to the unoccupied fullerene molecular orbitals ($\Delta_{Ba}^{E_{ionic}}$), covalent bonding between the Ba 5d and C_{60}-π* orbitals ($\Delta_{Ba}^{E_{covalent}}$) and metal−metal bonding between the Ba atoms ($\Delta_{Ba}^{E_{Ba-Ba}}$). Moreover, the fullerenes undergo small geometrical distortions from icosahedral symmetry in the formation of the clusters ($\Delta_{Ba}^{E_{geo}}$). Thus, we assumed

$$\Delta_{Ba}^{E} = \Delta_{Ba}^{E_{ionic}} + \Delta_{Ba}^{E_{covalent}} + \Delta_{Ba}^{E_{Ba-Ba}} + \Delta_{Ba}^{E_{geo}} \qquad (3)$$

$\Delta_{Ba}^{E_{geo}}$ is easy to calculate and varied between 2.3 to 6.6 kcal/mol. A systematic trend could not be observed. The Ba 5d orbitals are involved in both the Ba−Ba and covalent Ba—C_{60} bonding. Hence, a single-point energy calculation where the Ba 5d orbitals have been removed from the basis set should yield approximately the ionic bonding energy. For large *n* however, the 6s orbitals also participate in Ba−Ba bonding, thus this approximation becomes less valid as *n* increases. To estimate $\Delta_{Ba}^{E_{Ba-Ba}}$ separately, we performed energy calculations on Ba_n clusters whose coordinates were fixed to be equivalent to those in the $Ba_n(C_{60})_2$ clusters. The $\Delta_{Ba}^{E_{Ba-Ba}}$ var-

ied between −1.8 to −6.0 kcal/mol and once again no systematic trend could be found. $\Delta_{Ba}^{E_{covalent}}$ was obtained by subtracting the geometrical, Ba−Ba and ionic bonding energies from the total bonding energy. Our approximations include various reorganization effects. For instance, the $\Delta_{Ba}^{E_{Ba-Ba}}$ term as it is calculated here refers to a neutral Ba cluster whereas in the metal—C_{60} systems charge is transferred to the C_{60} moieties which will affect $\Delta_{Ba}^{E_{Ba-Ba}}$ to some extent. Likewise, the $\Delta_{Ba}^{E_{covalent}}$ term also contains the change of the bonding within each Ba_n cluster upon removal of some electronic charge due to Ba → C_{60} donation and other electronic reorganization effects. Moreover, in the systems *with* back-donation, $\Delta_{Ba}^{E_{ionic}}$ could be somewhat different. There is obviously no unique way how the total bonding energy may be split up into different contributions. We believe that our analysis is meaningful within its limitations posed by the approximations that were made and that it offers insight into the different modes of bonding present in the $Ba_n(C_{60})_2$ clusters.

Figure 11 shows the important $\Delta_{Ba}^{E_{ionic}}$ and $\Delta_{Ba}^{E_{covalent}}$ contributions, along with the average Mulliken charge per Ba. Note that the Δ_{Ba}^{E} are slightly different than those shown in Figure 9 since they were obtained using the higher integration accuracy. For $1 \leq n \leq 3$, the dominant interaction is ionic bonding. The magnitude of $\Delta_{Ba}^{E_{ionic}}$ decreases steadily with increasing n, as does the average charge per metal atom. However, the magnitude of $\Delta_{Ba}^{E_{covalent}}$ increases with increasing n, being the dominant interaction for $n = 5, 6$. For $n = 4$, $\Delta_{Ba}^{E_{ionic}} \approx \Delta_{Ba}^{E_{covalent}}$. This can be understood by noting that for large n full electron donation to the unoccupied fullerene orbitals cannot occur since the electrostatic repulsion between the Ba^{2+} ions would be too large for the cluster to be stable. Instead, as n increases so does back-donation to the Ba 5d orbitals, stabilizing clusters where all of the Ba atoms are located between the two fullerenes. Thus, the d-element character of Ba is essential when attempting to rationalize the structural features of these clusters.

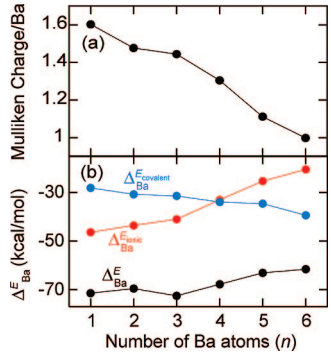

Figure 11. (a) average Mulliken charge per Ba and (b) relevant contributions to Δ_{Ba}^{E}, for the most stable $Ba_n(C_{60})_2$ ($1 \leq n \leq 6$) clusters.

The Δ_{Ba}^{E} data confirm that $Ba_3(C_{60})_2$ is energetically the most stable cluster. Its stability results from a balance mainly between two reverse trends: on the one hand a decreasing cluster stabilization from the Ba → C_{60} electron transfer and on the other hand an increasing stability from C_{60} → Ba back-donation, as n increases. However, the Δ_{Ba}^{E} of $Ba(C_{60})_2$ is only 1.1 kcal/mol higher. To explain the magic character of $Ba_3(C_{60})_2$, one needs to take entropic and enthalpic contributions into consideration. This will be done in the following section.

The Gibbs Free Energy of $Ba_n(C_{60})_2$ ($1 \leq n \leq 6$) Clusters. In an equilibrium mixture at constant temperature T and pressure p, it is ultimately the GFE of a species x, $G(x)$, which determines the stability of a given structure. The GFE is defined as

$$G(x) = H(x) - TS(x) \tag{4}$$

Here $H(x)$ and $S(x)$ are the enthalpy and entropy at the given temperature and pressure. The former is a sum of the energy of the species at 0 K plus a finite temperature enthalpy contribution,

$$H(x) = E(x) + H_{EC}(x) \tag{5}$$

Both $H_{EC}(x)$ and $S(x)$ are a sum of terms arising from rotational, translational, vibrational, and electronic degrees of freedom and the former includes the zero-point energy correction as well as the PV term. Upon defining $\Delta_{M}^{H_{EC}}$ and $T\Delta_{M}^{S}$ as the change in the finite temperature enthalpy correction per metal atom and the change in entropy per metal atom multiplied by the temperature for the reaction given in eq 1, then Δ_{M}^{G} may be written as

$$\Delta_{M}^{G} = \Delta_{M}^{E} + \Delta_{M}^{H_{EC}} - T\Delta_{M}^{S} \tag{6}$$

In the previous section we considered the first term of eq 6, Δ_{Ba}^{E}. Within this section we will analyze the last two terms and finally the Δ_{Ba}^{G} itself.

Figure 12a shows that $-T\Delta_{Ba}^{S}$ decreases with increasing n, implying that the entropic contribution to the Δ_{Ba}^{G} destabilizes larger clusters to a lesser extent than smaller ones. To understand why this should be the case consider the two limitting cases:

$$2n(C_{60}) + n\text{Ba} \rightarrow Ba_n(C_{60})_2 + (2n-2)C_{60} \tag{7}$$

$$2n(C_{60}) + n\text{Ba} \rightarrow n(Ba(C_{60})_2) \tag{8}$$

The first reaction yields the largest possible Ba—C_{60} cluster along with $(2n - 2)$ free C_{60}s, a total of $2n - 1$ molecules. The second produces n molecules, which are also the smallest possible Ba—C_{60} clusters. Clearly, the first reaction is entropically more favorable, since a greater amount of molecules are produced. This explains the experimental observation that larger clus-

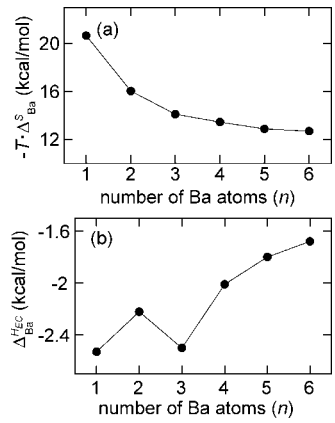

Figure 12. (a) $-T\Delta^S_{Ba}$ and (b) $\Delta^{H_{EC}}_{Ba}$, at 150 K and 10^{-6} Torr (the experimental pressure) for the most stable $Ba_n(C_{60})_2$ ($1 \leq n \leq 6$) clusters.

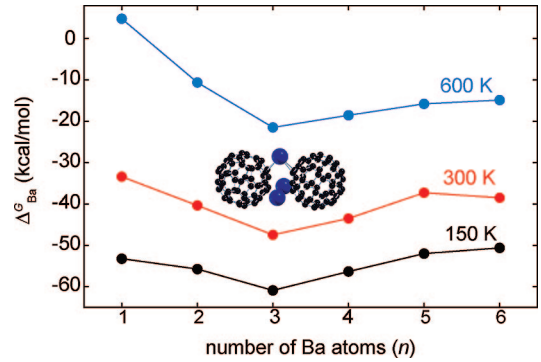

Figure 13. Δ^G_{Ba} at 150, 300, and 600 K and 10^{-6} Torr (the experimental pressure) for the most stable $Ba_n(C_{60})_2$ ($1 \leq n \leq 6$) clusters. The $n = 3$ cluster, also shown, has the lowest Δ^G_{Ba} at all temperatures considered.

ters became more abundant at elevated temperatures. In fact at the highest temperatures attained before fragmentation of all of the clusters occurred, only $Ba_{13}(C_{60})_6$ and $Ba_{14}(C_{60})_7$ were observed in the mass spectrum. This leads to the idea that entropic effects may be exploited to produce nanoscale clusters with highly desirable properties by adjusting the temperature of the heating stage.

In general $\Delta^{H_{EC}}_{Ba}$ becomes less negative with increasing n, as can be seen in Figure 12b. The only exception is that $\Delta^{H_{EC}}_{Ba}$ ($Ba_3(C_{60})_2$) $\approx \Delta^{H_{EC}}_{Ba}$ ($Ba(C_{60})_2$). The finite temperature enthalpy correction stabilizes smaller clusters, however it is about an order of magnitude smaller than the entropic term (at 150 K) and therefore does not have a substantial effect on the total Δ^G_{Ba}.

The total Δ^G_{Ba} given in Figure 13 shows that at the experimental pressure of 10^{-6} Torr and at temperatures ranging from 150 to 600 K, $Ba_3(C_{60})_2$ is magic. If we allow for uncertainties in the calculated entropy per metal atom by only up to 4%, the temperature at which all of the clusters will decompose (*i.e.*, where $\Delta G \approx 0$), is in agreement with experimental observations. Errors of this magnitude in ΔS are to be expected because the harmonic approximation has been applied and because small errors in the entropy inflate errors in the GFE (S is multiplied by T). Therefore we cannot reliably predict which cluster is the most stable at the highest annealing temperatures reached. Nonetheless, our results clearly underline the importance of calculating the enthalpic and, even moreso, entropic contributions to the GFE when determining absolute and relative cluster stabilities. For example, the Δ^E_{Ba} indicate that the relative order of stabilities is $n = 3 > 1 > 2 > 4 > 5 > 6$, whereas at 300 and 600 K the order becomes $n = 3 > 4 > 2 > 6 > 5 > 1$ and $n = 3 > 4 > 5 > 6 > 2 > 1$. The Δ^G_{Ba} values at 150 K indicate that already at this temperature $Ba_3(C_{60})_2$ should be magic, whereas experimentally $Ba_2(C_{60})_2$ is observed to have the highest abundance. This is likely because higher annealing temperatures are necessary to overcome the activation barrier to fragment the initial metastable clusters formed at the source. Only when this has occurred do the measurements probe the thermodynamic stability of the clusters.

The calculations show that the $Ba_n(C_{60})_2$ clusters have many local minima, which are all very close in energy to each other, differing only in a rotation of the C_{60}s around the metal core. This suggests that perhaps configurational entropy is also important in determining the absolute stability of the clusters. Since the configurational entropy for the free C_{60}s and metal atoms is zero, the change in configurational entropy per metal atom, $\Delta^{S_{conf}}_{Ba}$, for the reaction in eq 1 is given as

$$\Delta^{S_{conf}}_{Ba} = (k_B \ln \Omega)/n \qquad (9)$$

where Ω is the number of configurations and k_B is the Boltzmann constant. It is unclear how one may determine Ω, and instead we will calculate the amount of configurations necessary to have a noticeable impact on the total entropy. We find that Ω should be approximately equal to 29, 821, and 3.71×10^{14} to change $T\Delta^{S_{conf}}_{Ba}$ by 1, 2, and 10 kcal/mol, respectively, at 150 K. At higher temperatures, these numbers decrease; however, it is unlikely that inclusion of $\Delta^{S_{conf}}_{Ba}$ would affect the total Δ^G_{Ba} by more than a few kcal/mol. For the Ba clusters at 150, 300, and 600 K this will not change the order of stability.

Bonding and Stability of $K_n(C_{60})_2$ ($1 \leq n \leq 6$) Clusters. As we have shown, the favored bonding mode for potassium and barium to a single C_{60} was the same (configurations where the metal atom lay on top of a hexagonal fullerene face had the lowest Δ^E_M). This suggests that the two metals may also prefer the same geometries when bonding with two C_{60}s. Thus, for the $K_n(C_{60})_2$ clusters we have not optimized species which were found to be much higher in energy than the most stable $Ba_n(C_{60})_2$ clusters (**9.1**, **9.3**, **9.4**, and **9.6** in Figure 9). Instead, we have primarily focused on structures belonging to set A and set B as defined previously. We have optimized clusters containing σ_h or σ_v symmetry ele-

ments, and only those lowest in energy are shown in Figure 14, along with the Δ_K^E. Clearly, for ($1 \leq n \leq 4$) potassium bonds in a similar fashion as barium to the two C_{60}s. However, for $n = 5, 6$, geometries belonging to set B are preferred. For $n = 5$, the difference between the Δ_K^E for two sets is quite small, but it is seen to increase substantially for $K_6(C_{60})_2$.

To clarify the nature of the bonding we reoptimized the most energetically stable moieties with the higher integration accuracy, then performed a fragment orbital analysis, using the distorted C_{60}s and the K atoms as fragments. This analysis showed that the bonding is purely of an ionic nature, with an almost full transfer of the valence potassium $4s^1$ occupation to the LUMO of the C_{60}s. For $n = 1, 2$ analysis of the cluster orbitals confirmed that the HOMOs were composed solely of the fullerene LUMOs. For $n = 4, 6$ the highest $n/2$ orbitals and for $n = 3, 5$ the highest doubly occupied $(n - 1)/2$ orbitals plus the singly occupied HOMO (SOMO), consisted only of contributions from the unoccupied orbitals of the fullerenes.

As one might have expected, for large n the electron transfer from the potassium atoms to the C_{60} moieties is not complete because of the increasing Coulomb repulsion between the K^+ ions, see Figure 15. It should be noted that the same trend was also observed for K_nC_{60} clusters. We roughly estimated the purely electrostatic energy for the different clusters by assigning each atom the calculated Mulliken charge. We found that for $n = 3, 4$, the total electrostatic energy was more negative for the clusters from set A, whereas set B afforded lower electrostatic energies for $n = 5, 6$, indicating that the preferred geometries tend to minimize the total electrostatic energy. For large amounts of K, the clusters from the first set are less stable than those from the second because the close proximity of the positively charged K atoms results in an increased Coulomb repulsion. For the Ba clusters, on the other hand, the Ba d-element character compensates for this effect by allowing for a $C_{60} \rightarrow$ Ba back-donation of charge such that the clusters of set A remain the most stable at least up to $n = 6$.

Figure 15 illustrates that in general the Δ_K^E decreased in magnitude as n increased. These numbers are slightly different than those shown in Figure 14 since the geometries were reoptimized with a higher integration accuracy. A certain amount of energy is gained by transferring a K $4s^1$ occupation to the fullerene unoccupied orbitals. At the same time, the addition of more and more K atoms also results in an increase of the Coulomb repulsion between them. Hence, overall the energy gained by adding a K atom to the cluster decreases as n increases. Once again this finding correlates with the results obtained when clusters containing a single fullerene were considered. It must be pointed out that $K_4(C_{60})_2$ and $K_6(C_{60})_2$ were slightly more stable than $K_3(C_{60})_2$ and $K_5(C_{60})_2$, respectively. This is because clusters with $n = 4, 6$ afford an even number of electrons and hence a full electronic shell, whereas the valence shells for clusters with $n = 3, 5$ are only half-filled. Our calculations and those of others[10,11] show that for clusters containing one and two fullerenes, the K atoms prefer to be located on top of hexagonal faces. Thus, $K(C_{60})_2$ is more stable than $K_2(C_{60})_2$ because the K is situated directly between two hexagonal fullerene faces.

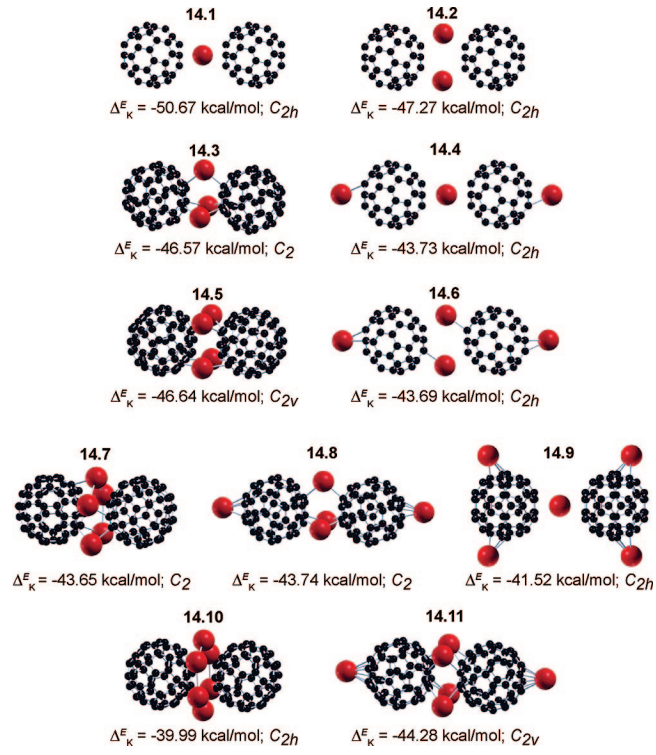

Figure 14. Optimized geometries and symmetries of the $K_n(C_{60})_2$ ($1 \leq n \leq 6$) clusters.

The Gibbs Free Energy of $K_n(C_{60})_2$ ($1 \leq n \leq 6$) Clusters. The vibrational frequencies for the most stable potassium clusters of a given n were calculated. This yielded the entropic, Figure 16a and enthalpic, Figure 16b contributions to the Δ_K^G. In general, the same trends were observed as for the barium clusters: the entropic term destabilized larger clusters to a lesser extent than smaller

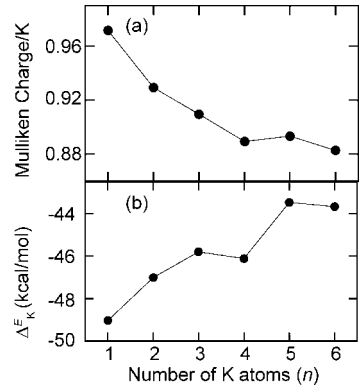

Figure 15. (a) Average Mulliken charge per K and (b) Δ_K^E, for the most stable $K_n(C_{60})_2$ ($1 \leq n \leq 6$) clusters.

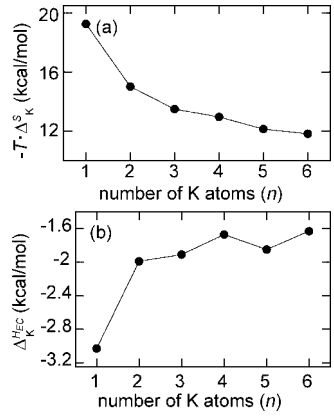

Figure 16. (a) $-T\Delta_K^S$ and (b) $\Delta_K^{H_{EC}}$, at 150 K and 10^{-6} Torr (the experimental pressure) for the most stable $K_n(C_{60})_2$ ($1 \leq n \leq 6$) clusters.

ones and the enthalpic term stabilized smaller clusters. However, at 150 K the latter term was about an order of magnitude smaller than the former and therefore did not substantially affect the total Δ_K^G, as was found for the Ba—C_{60} systems.

Once again we cannot accurately calculate the Δ_K^G at very high temperatures. However, at temperatures of 150 and 300 K along with the experimental pressure of 10^{-6} Torr the Δ_K^G in Figure 17 illustrates that $K_4(C_{60})_2$ is magic, in agreement with experiment. Here, even more so than for the Ba clusters, it is vital to take into account finite temperature effects when determining absolute and relative cluster stabilities. The most stable configurations at 0 K were $n = 1 > 2 > 4 > 3 > 6 > 5$, whereas at 150 and 300 K the order of stability was found to be $n = 4 > 3 > 2 > 6 > 5 > 1$ and $n = 4 > 6 > 5 > 3 > 2 > 1$, respectively. The results indicate that at higher temperatures, the entropy shifts the equilibrium to the formation of larger clusters. This is in agreement with experimental data indicating that only $K_{17}(C_{60})_7$ and $K_{14}(C_{60})_6$ are detected at the highest annealing temperatures reached. Previously, we indicated that the configurational entropy may contribute around 1−2 kcal/mol to the total Δ_M^G. For the Ba clusters such changes were deemed unimportant in determining the order of stability; however, this might not be the case

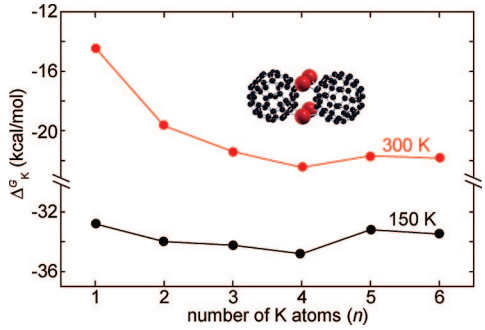

Figure 17. Δ_K^G at 150 and 300 K and 10^{-6} Torr (the experimental pressure) for the most stable $K_n(C_{60})_2$ ($1 \leq n \leq 6$) clusters. The $n = 4$ cluster, also shown, has the lowest Δ_K^G at both of these temperatures.

for the K clusters since the Δ_K^G are all closer in energy. Nonetheless, the calculated results are in-line with experiment, suggesting that configurational entropy does not have a major influence on the total GFEs or that $\Delta_K^{S_{conf}}$ is approximately the same for the different clusters.

CONCLUSIONS

A novel heating method was used to study the thermal stability of Ba−C_{60} and K−C_{60} compound clusters. The most stable systems produced could not be rationalized in terms of geometric or electronic shell-filling arguments. Our results demonstrate that the experimental setup can drastically influence if magic clusters are formed. When photon absorption is used to heat the cluster beam, metastable structures may be created. For the setup employed herein, it was found that lower annealing temperatures first yield information about the kinetic stability of the clusters. That is, temperatures exceeding the activation barrier necessary for the fragmentation of all of the initial metastable clusters formed at the source must first be reached before the thermodynamic stability of the clusters can be probed. The long annealing times allow the clusters to attain thermodynamic equilibrium, and therefore the most stable systems correspond to minima in the GFE at the given temperature and pressure. Due to entropic effects, raising the annealing temperature promotes the formation of larger species. This leads to the possibility of rationally engineering the production of nanoscale clusters with highly desirable properties by adjusting the temperature of the heating stage.

Density functional calculations have been performed to determine the energetically most stable structures for $M_n(C_{60})_2$ (M = Ba, K; $1 \leq n \leq 6$) clusters. For Ba, the most stable structural alternatives contained the metal sandwiched between the two fullerenes (set A). Ionic bonding, arising from an incomplete transfer of the valence occupations to the unoccupied fullerene orbitals was found to be the dominant bonding mechanism for small n . As n increased, covalent bonding between the Ba 5d and C_{60}-π^* orbitals increased, being the dominant bonding mechanism for $n = 5, 6$. This occurred as a result of $C_{60} \rightarrow$ Ba back-donation into the empty Ba 5d orbitals. Metal−metal bonding between the Ba atoms was also found; however, the associated energy was about an order of magnitude smaller than for the aforementioned bonding mechanisms. Thus, for the barium clusters the energetically most stable structures and their geometries are primarily determined by an interplay between ionic and covalent bonding. On the other hand, the $K_n(C_{60})_2$ ($1 \leq n \leq 6$) clusters exhibited only ionic bonding arising from a transfer of the $4s^1$ valence occupation into unoccupied C_{60} orbitals. The most stable geometries were found to minimize the total electrostatic energy. For $1 \leq n \leq 4$ isomers from

set A were the most stable, whereas for $n = 5, 6$, set B afforded structures with lower energies.

An analysis of the finite temperature contributions to the Δ_M^G revealed that the entropic term tends to destabilize larger clusters to a lesser extent than smaller ones. This could be explained by noting that a reaction yielding a single large cluster and many free fullerene molecules has a less negative entropy than one forming many small clusters and no or few free C_{60}s. The enthalpic term was seen to stabilize small clusters; however, at temperatures above 100 K it was about an order of magnitude smaller compared to the entropic term. Calculation of thermodynamic quantities was shown to be essential in determining the absolute and relative stabilities of these systems. Because of the formidable computational cost involved in the calculation of vibrational frequencies for such large systems, currently only a few studies, for example refs 22–24, are available which specifically consider the GFEs in determining absolute cluster (oligomer) stability.

We have also proposed a simple criterion (see Appendix) which may be used to unambiguously determine the most stable cluster while simultaneously revealing the order of stability of systems with the general formula A_nB_k where the quantity of only one of the elements changes. This criterion should be useful in analyzing the results of first-principles studies of binary and even multicomponent clusters.

METHODS

Experimental Methods. The experiments presented herein have been performed using a high-resolution reflectron TOF.[33] The clusters are formed within a noble gas condensation cell and transported through the system to the detector by a jet of He atoms. A novel heating/cooling stage allowing an adjustment to the cluster temperature between 150 and 1800 K is mounted directly after the cluster source.[34] Inside the stage the clusters thermalize with the He bath by collisions, thus assuming the desired temperature. The dwell time of the clusters inside the heating stage can be varied between 0.5 and 1 ms by controlling the He pressure inside the source. In all of the experiments the clusters were cooled to 150 K after exiting the heating stage and before photoionization. The setup is similar to Borggreen's[35] with the main difference being the maximum possible annealing temperature. Details of the experiment have been published elsewhere.[34,36]

Computational Methods. The computations were performed with the Amsterdam Density Functional (ADF)[18,37] and the Turbomole[38] program packages. The ADF code was used to obtain geometries and bonding energies, and to perform the bonding energy analyses in terms of fragment orbitals. Additional finite-temperature enthalpic and entropic contributions to the GFE were calculated with the Turbomole code at a somewhat lower level of theory. For the systems containing an even number of electrons, when a given symmetry constraint arose in a half-filled HOMO, a symmetry breaking distortion was applied to the cluster, resulting in a geometry with a closed-shell electronic configuration, unless stated otherwise. When an odd number of electrons were present, the structures presented here afford a single unpaired valence electron (doublet) and unrestricted DFT calculations were performed.

In the ADF calculations we have applied the revised Perdew–Burke–Ernzerhof (PBE) nonhybrid gradient density functional[39–42] along with the Vosko–Wilk–Nusair[43] (VWN) local density approximation (LDA). Full geometry optimizations were carried out employing a valence triple-ζ Slater-type basis set with polarization functions for all atoms (TZP) from the ADF basis set library. The core–shells up to 1s, 4p, and 2p of carbon, barium, and potassium, respectively, were kept frozen. Despite the fact that C and K are not heavy nuclei, all geometry optimizations with ADF were performed using the zeroth-order regular approximation (ZORA) Hamiltonian[44–46] in order to facilitate comparison with the "relativistic" Ba containing clusters. Initial geometry optimizations employing an integration accuracy of 4 were performed to determine the most stable $M_n(C_{60})_2$ (M = K, Ba, $1 \leq n \leq 6$) structures for a given n . Afterward computations with an integration accuracy of 6 were carried out to obtain a more precise energy ordering between the most stable clusters for a given n. To clarify the nature of the bonding, we performed a fragment orbital analysis, using the distorted fullerenes (as found in the optimized clusters) and the free metal atoms, as fragments.[18] This yielded the composition of the molecular orbitals of the metal-fullerene cluster in terms of the occupied and unoccupied orbitals of Ba/K and C_{60}.

It was computationally too expensive to perform numerical–derivative frequency calculations with ADF. Therefore, to reduce the computational effort, the ADF geometries were reoptimized with Turbomole, using the "resolution-of-identity" (RI)[47,48] technique along with the polarized split-valence SV(P) basis set augmented with the default auxiliary (RI) basis sets from the Turbomole basis set library. The PBE[39,49–51] functional was employed, since the revPBE was not available. Relativistic effects were considered in these calculations *via* a scalar relativistic (6s6p5d)/[4s3p3d] ECP basis with 46 core–electrons.[38,52] Using the SV(P) basis and the RI technique, it was possible to perform analytical calculations of the vibrational frequencies[53,54] and finite-temperature contributions to the GFE based thereupon. At times, it was necessary to lower the symmetry and reoptimize the cluster geometry in order to obtain minima. However, the energy changes were much smaller than the bonding energy differences obtained from ADF and Turbomole and are most likely explained by the different basis sets applied and the use of the RI technique. These cluster geometries were not reoptimized with ADF due to the immense computational cost involved. The Δ_M^E and Δ_M^G (see eq 2) presented were obtained by using the ADF energies (which should be considered more accurate than those obtained with Turbomole because of the higher quality basis set applied), augmented with the finite temperature corrections from the Turbomole frequencies calculations. Thermochemical properties were calculated using standard expressions. Because it was computationally too expensive to perform frequency calculations on all of the systems considered, we assumed that the clusters which have the lowest energy will also have the lowest Gibbs free energy. Other affordable methods could not provide superior results: molecular dynamics (MD) requires the use of unknown interaction potentials and *ab initio* MD would be prohibitively expensive. A subset of the graphics were prepared using the XCrySDen program.[55]

APPENDIX

For systems containing a single element, a comparison of the binding energy per atom easily reveals which clusters are magic. However, currently there is no suitable criterion available which may be used to gauge the absolute or relative stability of systems with the general formula A_nB_k where n varies. In the past, fragmentation energies,[25–27] averaged binding energies,[2,26,27] or the second difference in binding energies[2] were employed. Herein, we examine these criteria showing that in unfavorable circumstances they may lead to contradictory or incorrect conclusions. We propose a new criterion and prove that it allows for an easy and unambiguous determination of the most stable cluster while simultaneously revealing the order of stability of systems with the general formula A_nB_k. It is assumed that these clusters may react with free A, B and other A_mB_k species. The criterion can

also be applied to evaluate the stabilities of multicomponent systems ($A_nB_kC_l$, $A_nB_kC_lD_p$, *etc.*) as long as the quantity of only one of the elements changes.

For a set of clusters with the general formula A_nB_k where n varies and k is constant consider the change in W per varied component, Δ_A^W, defined as

$$\Delta_A^W(A_nB_k) = \frac{W(A_nB_k) - nW(A) - kW(B)}{n} \quad (10)$$

where W(A) may denote the energy, E, enthalpy, H, Gibbs free energy, G, or the Helmholz free energy of species A, depending on whether finite temperature and/or pressure effects are important for the system under consideration. If A_mB_k is thermodynamically more stable than A_nB_k the reaction

$$xA_nB_k + (yk - xk)B \rightarrow yA_mB_k \quad (11)$$

with $xn = ym$ will be exergonic, *i.e.*,

$$\Delta W = yW(A_mB_k) - xW(A_nB_k) - (yk - xk)W(B) < 0 \quad (12)$$

Rearranging eq 10 we find

$$W(A_nB_k) = n\Delta_A^W(A_nB_k) + nW(A) + kW(B) \quad (13)$$

and a similar expression for $W(A_mB_k)$. Substituting these into eq 12 and using the fact that mass balance in eq 11 requires that $ym = xn$ yields

$$\Delta_A^W(A_mB_k) < \Delta_A^W(A_nB_k) \quad (14)$$

Thus, a comparison of the Δ_A^W of two different clusters will automatically determine if the reaction in eq 11 is thermodynamically favorable and therefore identifies the most stable cluster. Since this holds for any m and any n, a comparison of the Δ_A^W values of a set of clusters will unambiguously elucidate which cluster is magic (the one with the most negative Δ_A^W) as well as yield the relative order of stabilities. We note that a similar proof can be constructed for a multicomponent system as long as Δ_A^W is defined as

$$\Delta_B^W(A_nB_kC_l...) = \frac{W(A_nB_kC_l...) - nW(A) - kW(B) - lW(C) - ...}{n} \quad (15)$$

where n varies and k, l, ... remain constant.

Common criteria for identifying magic clusters include maxima in the fragmentation energies defined as[25−27]

$$D(n,\ n-1) \equiv E_F = -E(A_nB_k) + E(A) + E(A_{n-1}B_k), \quad (16)$$

maxima in the averaged binding energies given by[2,26,27]

$$E_{B_{av}}(A_nB_k) = \frac{kE(B) + nE(A) - E(A_nB_k)}{n+k}, \quad (17)$$

or minima in the second difference in binding energies calculated *via*[2]

$$\Delta^2E_B(A_nB_k) = E_B(A_nB_k) - 0.5[E_B(A_{n-1}B_k) + E_B(A_{n+1}B_k)]. \quad (18)$$

To demonstrate how these criteria may fail under unfortunate circumstances, let us assume that our calculations showed that **9.1**, **9.5**, **9.8**, **9.10**, **9.12**, and **9.14** in Figure 9 were found to be the most stable $Ba_n(C_{60})_2$ clusters for a given n . That is, for the sake of discussion we assume for the moment that **9.2** does not exist and determine which clusters are predicted to be magic by the different criteria. Table 2 shows that the fragmentation energies and second difference in binding energies indicate that $Ba_2(C_{60})_2$ is magic, whereas the averaged binding energies predict $Ba_6(C_{60})_2$ to be particularly stable. The Δ_{Ba}^E values, on the other hand, indicate that $Ba_3(C_{60})_2$ has enhanced stability. However, for the reactions

$$3Ba_2(C_{60})_2 \rightarrow 2Ba_3(C_{60})_2 + 2C_{60} \quad (19)$$

$$Ba_6(C_{60})_2 + 2C_{60} \rightarrow 2Ba_3(C_{60})_2 \quad (20)$$

ΔE is −22.50 and −68.01 kcal/mol, respectively. In both cases the products are more stable than the reactants clearly indicating that $Ba_2(C_{60})_2$ and $Ba_6(C_{60})_2$ cannot be magic. Here, the E_F and Δ^2E_B values fail to make the right prediction because $Ba(C_{60})_2$ (**9.1**) is much less stable than $Ba_2(C_{60})_2$ (**9.5**).

Now, assuming that our calculations also included **9.2** then, with the exception of the averaged binding energies, all of the methods would indicate that $Ba_3(C_{60})_2$ is magic. The E_F values would exhibit maxima for the $n = 1, 3, 6$ clusters and the Δ^2E_B values would show minima for $n = 1, 3$. The $E_{B_{av}}$ would once again predict that the largest cluster, $Ba_6(C_{60})_2$, is the most stable, which we have shown previously cannot be the case. However, neither the E_F values nor the Δ^2E_B values are able to determine the relative order of stability of these systems. The E_F simply determines the exothermicity of the following reaction: $A_nB_k \rightarrow A + A_{n-1}B_k$, whereas the Δ^2E_B compares the binding energy of the cluster A_nB_k with the average of the binding energies of $A_{n+1}B_k$ and $A_{n-1}B_k$. Therefore, these criteria are commonly used only to determine the most stable cluster and not to determine the relative order of stabilities.

Thus, in this particular case the distribution of energies among the clusters is such that fortunately all methods, except the $E_{B_{av}}$, pick the same magic cluster. However, only the measure proposed herein can be used to determine the order of the stabilities of the clusters within the set. As we have shown, if **9.2** is not within the set of clusters, and instead one considers a much less stable $Ba(C_{60})_2$ isomer, then none of the commonly used criteria correctly identifies the most stable cluster.

As we have already indicated a comparison of the Δ_A^W values for a set of clusters, A_nB_k, can be used to determine the most stable cluster, as well as the relative order of stabilities, as long as only n varies. However, under certain circumstances it may be possible to determine which cluster is magic for varying n and k . For example, say for two sets of clusters, A_3B_k and A_6B_k, we find that A_3B_4 and A_6B_4 have the lowest Δ_B^W values. A comparison of Δ_A^W values for these two clusters could then be used to determine the most stable system.

Studies of binary, ternary, and in general multicomponent clusters are currently of great interest because such materials may possess novel magnetic properties[28,29] and be used as hydrogen storage media, [30] free-standing quantum dots,[31] and building blocks for nanomaterials.[32] We believe

TABLE 2. A Comparison of the Different Criteria Used To Determine Enhanced Cluster Stability for $Ba_n(C_{60})_2$ Clusters. The Values Given in Bold Indicate the Clusters Predicted To Be Magic by the Specified Criteria[a]

n	structure[b]	E_F[c]	Δ^2E_B[d]	$E_{B_{av}}$[e]	Δ_{Ba}^E[f]
1	**9.1**	28.28	41.20	9.43	−28.28
2	**9.5**	**110.69**	**−14.98**	34.74	−69.48
3	**9.8**	80.74	−12.65	43.94	**−73.23**
4	**9.10**	55.43	−5.57	45.86	−68.78
5	**9.12**	44.29	3.83	45.63	−63.89
6	**9.14**	51.96		**46.42**	−61.90

[a] All values given in kcal/mol for A_nB_k clusters with A = Ba and $1 \leq n \leq 6$, B = C_{60}, $k = 2$. [b] Illustrated in Figure 9. [c] Fragmentation energies as defined in eq 16. [d] Second difference in binding energies as defined in eq 18. [e] Averaged binding energies as defined in eq 17. [f] Binding energies per barium atom as defined in eq 10.

our criterion will be particularly useful for analyzing the results obtained from first-principles calculations on these increasingly important systems.

Acknowledgment. E. Zurek acknowledges financial support from the "International Max-Planck Research School for Advanced Materials" (IMPRS-AM). J. Autschbach acknowledges support from the Center of Computational Research at SUNY Buffalo and is grateful for financial support from the CAREER program of the National Science Foundation (Grant No. CHE-0447321).

Supporting Information Available: Cartesian coordinates and energies of the M_nC_{60} ($M = K$, $1 \leq n \leq 6$ and $M = Ba$, $1 \leq n \leq 3$) and $M_n(C_{60})_2$ ($M = K, Ba$; $1 \leq n \leq 6$) clusters studied by density functional theory. This material is available free of charge *via* the Internet at http://pubs.acs.org.

REFERENCES AND NOTES

1. Enders, A.; Malinowski, N.; Ievlev, D.; Zurek, E.; Autschbach, J.; Kern, K. Magic Alkali-Fullerene Compound Clusters of Extreme Thermal Stability. *J. Chem. Phys.* **2006**, *125*, 191102.
2. Chen, Z. F.; Neukermans, S.; Wang, X.; Janssens, E.; Zhou, Z.; Silverans, R. E.; King, R. B.; Schleyer, P. v. R.; Lievens, P. To Achieve Stable Spherical Clusters: General Principles and Experimental Confirmations. *J. Am. Chem. Soc.* **2006**, *128*, 12829–12834.
3. Neukermans, S.; Janssens, E.; Chen, Z. F.; Silverans, R. E.; Schleyer, P. v. R.; Lievens, P. Extremely Stable Metal-Encapsulated $AlPb_{10}^+$ and $AlPb_{12}^+$ Clusters: Mass Spectrometric Discovery and Density Functional Theory Study. *Phys. Rev. Lett.* **2004**, *92*, 163401.
4. Veldeman, N.; Höltzl, T.; Neukermans, S.; Veszprémi, T.; Nguyen, M. T.; Lievens, P. Experimental Observation and Computational Identification of $Sc@Cu_{16}^+$, a Stable Dopant-Encapsulated Copper Cage. *Phys. Rev. A* **2007**, *76*, 011201(R)
5. Cui, L.-F.; Huang, X.; Wang, L.-M.; Li, J.; Wang, L.-S. Endohedral Stannaspherenes $M@Sn_{12}^-$: A Rich Class of Stable Molecular Cage Clusters. *Angew. Chem., Int. Ed.* **2007**, *46*, 742–745.
6. Dognon, J.-P.; Clavaguéra, C.; Pyykkö, P. Towards a 32-Electron Principle: $Pu@Pb_{12}$ and Related Systems. *Angew. Chem., Int. Ed.* **2007**, *46*, 1427–1430.
7. Zimmermann, U.; Malinowski, N.; Näher, U.; Frank, S.; Martin, T. P. Multilayer Metal Coverage of Fullerene Molecules. *Phys. Rev. Lett.* **1994**, *72*, 3542–3545.
8. Martin, T. P.; Malinowski, N.; Zimmermann, U.; Näher, U.; Schaber, H. Metal-Coated Fullerene Molecules and Clusters. *J. Chem. Phys.* **1993**, *99*, 4210–4212.
9. Bergeron, D. E.; Roach, P. J.; Castleman, A. W.; Jones, N.; Khanna, S. N. Al Cluster Superatoms as Halogens in Polyhalides and as Alkaline Earths in Iodide Salts. *Science* **2005**, *307*, 231–235.
10. Weis, P.; Beck, R. D.; Bräuchle, G.; Kappes, M. M. Properties of Size and Composition Selected Gas Phase Alkali Fulleride Clusters. *J. Chem. Phys.* **1994**, *100*, 5684–5695.
11. Hamamoto, N.; Jitsukawa, J.; Satoko, C. Electronic and Geometric Properties of Alkali-C_{60} Molecules. *Eur. Phys. J. D.* **2002**, *19*, 211–221.
12. Östling, D.; Rosén, A. Electronic Structure and Optical Properties of Bare and Li, Na, K and Ca Coated C_{60} Molecule. *Chem. Phys. Lett.* **1997**, *281*, 352–359.
13. Gong, X. G.; Kumar, V. Metallic Coverings of Calcium on C_{60}. *Chem. Phys. Lett.* **2001**, *334*, 238–244.
14. Irle, S.; Zheng, G.; Wang, Z.; Morokuma, K. Theory-Experiment Relationship of the "Shrinking Hot Giant" Road of Dynamic Fullerene Self—Assembly in Hot Carbon Vapor. *Nano* **2007**, *2*, 21–30.
15. Pyykkö, P.; Wang, C.; Straka, M.; Vaara, J. A London—Type Formula for the Dispersion Interactions of Endohedral A@B Systems. *Phys. Chem. Chem. Phys.* **2007**, *9*, 2954–2958.
16. Scuseria, G. E. What is the Lowest-Energy Isomer of the C_{60} Dimer. *Chem. Phys. Lett.* **1996**, *257*, 583–586.
17. Zhou, P.; Dong, Z. H.; Rao, A. M.; Eklund, P. C. Reaction Mechanism for the Photopolymerization of Solid Fullerene C_{60}. *Chem. Phys. Lett.* **1993**, *211*, 337–340.
18. te Velde, G.; Bickelhaupt, F. M.; Baerends, E. J.; Fonseca Guerra, C.; van Gisbergen, S. J. A.; Snijders, J. G.; Ziegler, T. Chemistry with ADF. *J. Comput. Chem.* **2001**, *22*, 931–967.
19. Gagliardi, L.; Pyykkö, P. Cesium and Barium as Honorary *d* Elements: CsN_7Ba as an Example. *Theor. Chem. Acc.* **2003**, *110*, 205–210.
20. Pyykkö, P. Dirac-Fock One-Center Calculations. *J. Chem. Soc., Faraday Trans. 2* **1979**, *75*, 1256–1276.
21. Gagliardi, L. New Group 2 Chemistry: A Multiple Barium−Nitrogen Bond in the CsNBa Molecule. *J. Am. Chem. Soc.* **2002**, *124*, 8757–8761.
22. Zurek, E.; Woo, T. K.; Firman, T. K.; Ziegler, T. Modeling the Dynamic Equilibrium Between Oligomers of $(AlOCH_3)_n$ in Methylaluminoxane (MAO). A Theoretical Study Based on a Combined Quantum Mechanical and Statistical Mechanical Approach. *Inorg. Chem.* **2001**, *40*, 361–370.
23. Timoshkin, A. Y.; Schaefer, H. F. From Parasitic Association Reactions Toward the Stoichiometry Controlled Gas Phase Synthesis of Nanoparticles: A Theoretically Driven Challenge for Experimentalists. *Chem. Rec.* **2002**, *2*, 319–338.
24. Timoshkin, A. Y.; Schaefer, H. F. Spontaneous Gas—Phase Generation of Needle—Shaped Clusters Which Violate the Isolated Square Rule: A Facile Road to GaN Nanorods? *J. Am. Chem. Soc.* **2004**, *126*, 12141–12154.
25. Guo, P.; Ren, Z.-Y.; Yang, A.-P.; Han, J.-G.; Bian, J.; Wang, G.-H. Relativistic Computational Investigation: The Geometries and Electronic Properties of $TaSi_n^+$ (n = 1−13, 16) Clusters. *J. Phys. Chem. A* **2006**, *110*, 7453–7460.
26. Wang, J.; Han, J.-G. A Theoretical Study on Growth Patterns of Ni-Doped Germanium Clusters. *J. Phys. Chem. B* **2006**, *110*, 7820–7827.
27. Wang, J.; Han, J.-G. Geometries and Electronic Properties of the Tungsten-Doped Germanium Clusters: WGe_n (n = 1−17). *J. Phys. Chem. A* **2006**, *110*, 12670–12677.
28. Wang, J. L.; Bai, J. L.; Jellinek, J.; Zeng, X. C. Gold-Coated Transition-Metal Anion $[Mn_{13}@Au_{20}]^-$ with Ultrahigh Magnetic Moment. *J. Am. Chem. Soc.* **2007**, *129*, 4110–4111.
29. Wang, W.-G.; Zhou, A.-J.; Zhang, W.-X.; Tong, M.-L.; Chen, X.-M.; Nakano, M.; Beedle, C. C.; Hendrickson, D. N. Giant Heterometallic $Cu_{17}Mn_{28}$ Cluster with T_d Symmetry and High-Spin Ground State. *J. Am. Chem. Soc.* **2007**, *129*, 1014–1015.
30. Sun, Q.; Jena, P.; Wang, Q.; Marquez, M. First-Principles Study of Hydrogen Storage on $Li_{12}C_{60}$. *J. Am. Chem. Soc.* **2006**, *128*, 9741–9745.
31. Reboredo, F. A.; Galli, G. Theory of Alkyl-Terminated Silicon Quantum Dots. *J. Phys. Chem. B* **2005**, *109*, 1072–1078.
32. Cumberland, S. L.; Hanif, K. M.; Javier, A.; Khitrov, G. A.; Strouse, G. F.; Woessner, S. M.; Yun, C. S. Inorganic Clusters as Single-Source Precursors for Preparation of CdSe, ZnSe, and CdSe/ZnS Nanomaterials. *Chem. Mater.* **2002**, *14*, 1576–1584.
33. Branz, W. *The Structure of $(C_{60})_n$ Clusters*. Ph.D. Thesis. University of Stuttgart, Stuttgart, Germany, 2001.
34. Ievlev, D. N.; Küster, A.; Enders, A.; Malinowski, N.; Schaber, H.; Kern, K. A Combined Heating Cooling Stage for Cluster Thermalization in the Gas Phase. *Rev. Sci. Instrum.* **2003**, *74*, 3031–3034.
35. Borggreen, J.; Hansen, K.; Chandezon, F.; Dossing, T.; Elhajal, M.; Echt, O. Absolute Separation Energies for Na Clusters. *Phys. Rev. A* **2000**, *62*, 013202.
36. Branz, W.; Malinowski, N.; Enders, A.; Martin, T. P. Structural Transition in $(C_{60})_n$ Clusters. *Phys. Rev. B* **2002**, *66*, 094107.
37. Baerends, E. J.; Autschbach, J.; Bérces, A.; Bickelhaupt, F. M.; Bo, C.; Boerrigter, P. M.; Cavallo, L.; Chong, D. P.; Deng, L.; Dickson, R. M.; *et al.* ADF2006.01, SCM, Theoretical Chemistry, Vrije Universiteit, Amsterdam, The Netherlands, URL http://www.scm.com.
38. Ahlrichs. R. *Turbomole*, version 5.7; Quantum Chemistry Group, Universitaet Karlsruhe: Karlsruhe, Germany, 2004.

39. Perdew, J. P.; Burke, K.; Wang, Y. Generalized Gradient Approximation for the Exchange-Correlation Hole of a Many-Electron System. *Phys. Rev. B* **1996**, *54*, 16533–16539.
40. Zhang, Y.; Yang, W. Comment on Generalized Gradient Approximation Made Simple. *Phys. Rev. Lett.* **1998**, *80*, 890.
41. Perdew, J. P.; Burke, K.; Ernzerhof, M. Reply to Comment on Generalized Gradient Approximation Made Simple. *Phys. Rev. Lett.* **1998**, *80*, 891.
42. Hammer, B.; Hansen, L. B.; Norskov, J. K. Improved Adsorption Energetics within Density-Functional Theory using Revised Perdew−Burke−Ernzerhof Functionals. *Phys. Rev. B* **1999**, *59*, 7413–7421.
43. Vosko, S. H.; Wilk, L.; Nusair, M. Accurate Spin-Dependent Electron Liquid Correlation Energies for Local Spin Density Calculations: a Critical Analysis. *Can. J. Phys.* **1980**, *58*, 1200–1211.
44. van Lenthe, E.; Baerends, E. J.; Snijders, J. G. Relativistic Regular Two-Component Hamiltonians. *J. Chem. Phys.* **1993**, *99*, 4597–4610.
45. van Lenthe, E.; Baerends, E. J.; Snijders, J. G. Relativistic Total Energy Using Regular Approximations. *J. Chem. Phys.* **1994**, *101*, 9783–9792.
46. van Lenthe, E. The ZORA Equation. Ph.D. Thesis. Vrije Universiteit Amsterdam, Netherlands, 1996.
47. Eichkorn, K.; Treutler, O.; Öhm, H.; Häser, M.; Ahlrichs, R. Auxiliary Basis Sets to Approximate Coulomb Potentials. *Chem. Phys. Lett.* **1995**, *242*, 652–660.
48. Eichkorn, K.; Treutler, O.; Öhm, H.; Häser, M.; Ahlrichs, R. Auxiliary Basis Sets to Approximate Coulomb Potentials. *Chem. Phys. Lett.* **1995**, *240*, 283–289.
49. Dirac, P. A. M. Quantum Mechanics of Many-Electron Systems. *Proc. R. Soc. (London) A* **1929**, *123*, 714–733.
50. Slater, J. C. A Simplification of the Hartree−Fock Method. *Phys. Rev.* **1951**, *81*, 385–390.
51. Perdew, J. P.; Chevary, J. A.; Vosko, S. H.; Jackson, K. A.; Pederson, M. R.; Singh, D. J.; Fiolhais, C. Atoms, Molecules, Solids, and Surfaces: Applications of the Generalized Gradient Approximation for Exchange and Correlation. *Phys. Rev. B* **1992**, *46*, 6671–6687.
52. Kaupp, M.; Schleyer, P. v. R.; Stoll, H.; Preuss, H. Pseudopotential Approaches to Ca, Sr, and Ba Hydrides. Why are Some Alkaline Earth MX_2 Compounds Bent. *J. Chem. Phys.* **1991**, *94*, 1360–1366.
53. Deglmann, P.; May, K.; Furche, F.; Ahlrichs, R. Nuclear Second Analytical Derivative Calculations Using Auxiliary Basis Set Expansions. *Chem. Phys. Lett.* **2004**, *384*, 103–107.
54. Deglmann, P.; Furche, F.; Ahlrichs, R. An Efficient Implementation of Second Analytical Derivatives for Density Functional Methods. *Chem. Phys. Lett.* **2002**, *362*, 511–518.
55. Kokalj, A. XCrySDen—a New Program for Displaying Crystalline Structures and Electron Densities. *J. Mol. Graphics Modell.* **1999**, *17*, 176–179.